THE ASTROPHYSICAL JOURNAL, 494:194–201, 1998 February 10
© 1998. The American Astronomical Society. All rights reserved. Printed in U.S.A.

X-RAY AND OPTICAL SPECTROSCOPY OF IRAS 20181−2244: NOT A TYPE 2 QSO, BUT A I Zw 1 OBJECT

JULES P. HALPERN[1,2]
Columbia Astrophysics Laboratory, Columbia University, 550 West 120th Street, New York, NY 10027; jules@astro.columbia.edu
AND
EDWARD C. MORAN[1]
Institute of Geophysics and Planetary Physics, Lawrence Livermore National Laboratory, L-413, Livermore, CA 94450; edhead@jester.berkeley. edu
Received 1997 June 16; accepted 1997 September 15

ABSTRACT

We analyze new optical spectra of IRAS 20181−2244 that confirm its classification as a I Zw 1 object (or narrow-line Seyfert 1 galaxy), one of 20 such objects detected in the *ROSAT*/*IRAS* all-sky survey. *ASCA* X-ray data on IRAS 20181−2244 support this classification since they are fitted by a simple power-law spectrum of $\Gamma = 2.37 \pm 0.09$ that is typical of this class but steeper than that of ordinary Seyfert 1 or Seyfert 2 galaxies. Rapid X-ray variability is also observed in IRAS 20181−2244, ruling out a hidden/scattered QSO interpretation for this object. Its 0.5–10 keV luminosity is 5.5×10^{44} ergs s^{-1}, and its variability signifies an efficiency of at least 4% for conversion of gravitational energy to X-rays. We discuss the important differences between the I Zw 1 class and the "type 2 QSO," or high-luminosity Seyfert 2 galaxy. While I Zw 1 objects of QSO-like luminosity are ubiquitous in infrared, optical, and soft X-ray selected samples, type 2 QSOs are rare, and there is a dearth of evidence for even a single one in X-rays. It is not clear how this imbalance relates to unified models of AGNs.

Subject headings: galaxies: active — galaxies: individual (IRAS 20181−2244) — galaxies: Seyfert — infrared: galaxies — X-rays: galaxies

1. INTRODUCTION

The galaxy IRAS 20181−2244 ($z = 0.185$) was detected as an X-ray source in the *ROSAT* all-sky survey (Boller et al. 1992). We measure its position on the UK Schmidt sky survey to be (J2000) $20^h21^m4\overset{s}{.}4$, $-22°35'20''$. A finding chart is shown in Figure 1. Moran, Halpern, & Helfand (1996) obtained spectra and classifications of most of the Boller et al. sample, showing that IRAS 20181−2244 is one of 20 objects, comprising perhaps 10% of the sample, that could logically be grouped together as members of the I Zw 1 family. Named after the well-known prototype (e.g., Phillips 1976) with which they share a number of distinctive characteristics, I Zw 1 objects have unusually narrow permitted lines, strong permitted Fe II lines, and relatively weak forbidden lines. Also referred to as narrow-line Seyfert 1 galaxies (NLS1s) by Osterbrock & Pogge (1985) and Goodrich (1989), these objects with FWHM Hβ < 2000 km s^{-1} and [O III] λ5007/Hβ < 3, are different from type 2 Seyfert galaxies, which generally have [O III]/Hβ > 3 and no permitted Fe II lines. Not all NLS1s have very strong Fe II emission lines like I Zw 1, but since all 20 in the Moran et al. (1996) study have Fe II to some degree, we will refer to them here as I Zw 1 objects rather than NLS1s. This name avoids possible confusion with the terms "narrow-line QSO" or "type 2 QSO" that are often encountered in the literature as shorthand for the concept of a high-luminosity analog of a Seyfert 2 galaxy. Although Elizalde & Steiner (1994) proposed that IRAS 20181−2244 is, in fact, a type 2 QSO, we will show that its optical, X-ray, and infrared properties are typical of the I Zw 1 class, which includes other very luminous members (see e.g., Forster & Halpern 1996). We will discuss the important differences between I Zw 1 objects and the hypothetical type 2 QSOs and argue that there is very little evidence for the existence of *any* type 2 QSOs among X-ray selected samples.

2. OPTICAL SPECTROSCOPY

Optical spectra of IRAS 20181−2244 were obtained in 1994 July using the Goldcam CCD spectrometer on the KPNO 2.1 m telescope. Two different 600 lines mm^{-1} gratings were used to cover the wavelength range 3200–8500 Å at a resolution of $\approx$4.2 Å. Standard methods were used to extract the spectrum of the nucleus, determine the wavelength scale, correct the telluric absorption bands, and calibrate the flux. The composite of these spectra is shown in Figure 2, and line intensity measurements are given in Table 1. The dereddened line intensities were derived assuming a Galactic $E(B-V) = 0.12$ mag, based on the Stark et al. (1992) neutral hydrogen column density, $N_H = 7.4 \times 10^{20}$ cm^{-2} in this direction. As we will discuss below, there is likely additional reddening intrinsic to IRAS 20181−2244 that is not taken into account in Table 1.

The redshifts of the stronger lines listed in Table 1 show evidence of stratification in the emission-line regions. The higher ionization lines such as [Ne V] and [O III] are blueshifted from the lower ionization lines by as much as 150 km s^{-1}, a trend that is not uncommon among Seyfert galaxies. The differences are highly significant, as the peak wavelengths of the stronger lines can be measured almost as accurately as the calibration arc lines, the wavelength solution of which has an internal dispersion of 6–8 km s^{-1} across the entire spectrum.

Several features of this spectrum are noteworthy in support of our I Zw 1 classification. First is the presence of

[1] Visiting Astronomer.
[2] Visiting Astronomer, Kitt Peak National Observatory, National Optical Astronomy Observatories, which is operated by AURA, Inc., under a cooperative agreement with the National Science Foundation.

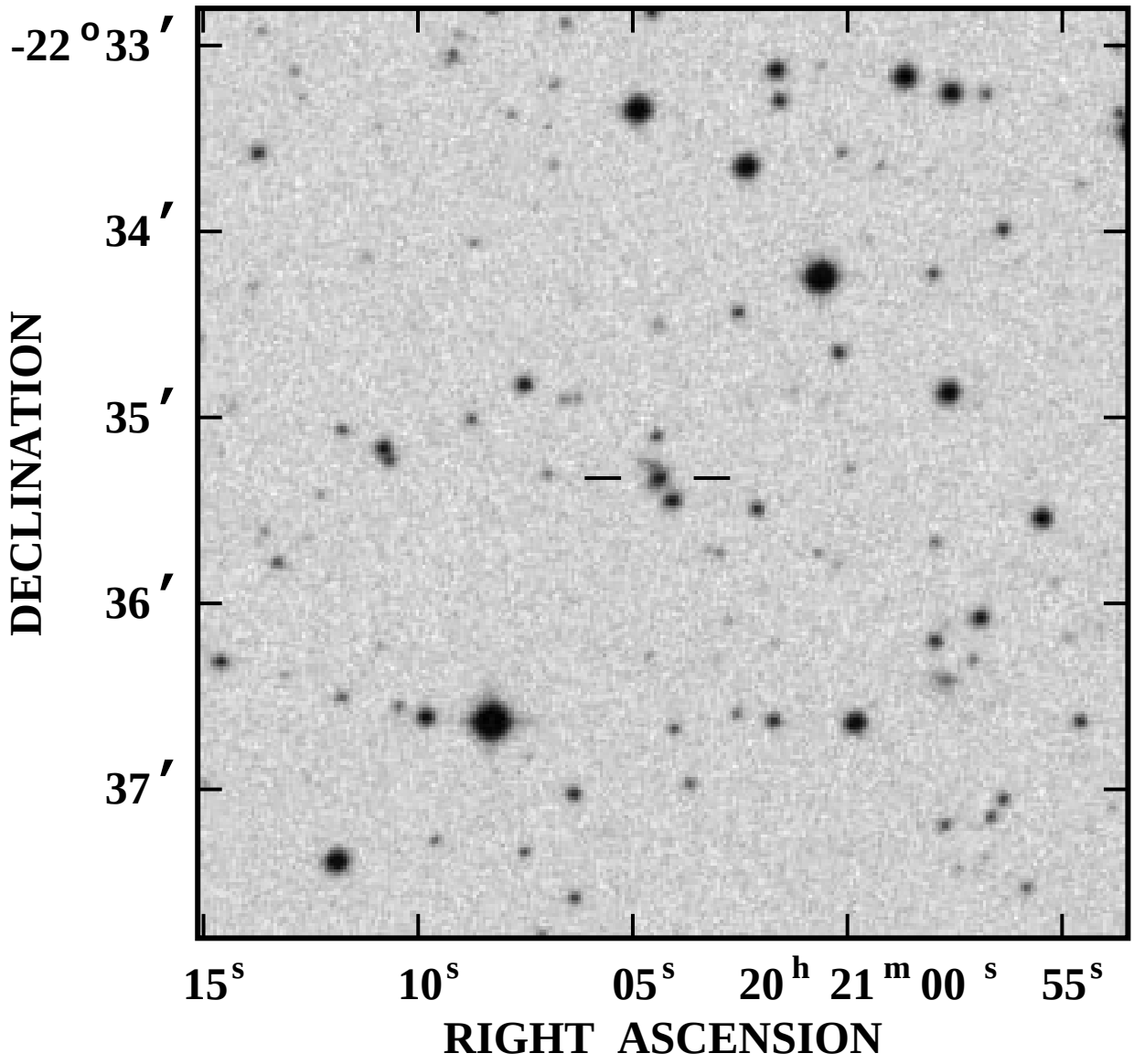

FIG. 1.—Finding chart for IRAS 20181−2244 from the digitized SERC Southern Sky Survey IIIa-J plate. Position of the galaxy is (J2000) $20^h21^m4\overset{s}{.}4$, −22°35′20″. This chart corrects the one given by Elizalde & Steiner (1994).

permitted Fe II lines. The Fe II blend around 4750 Å is measured to be $\simeq 0.7$ times the strength of Hβ. Second are the line profiles, which differ between permitted and forbidden lines. Although [O III] is actually broader than Hβ at half maximum (≈ 700 km s^{-1} for [O III] vs. ≈ 460 km s^{-1} for Hβ), the Balmer lines have broader wings, extending to at least ± 5000 km s^{-1} at zero intensity (see Figs. 3 and 4). This breadth is particularly clear in the case of Hα, which is not significantly contaminated by other lines in its wings. Unfortunately, it is not possible to make a detailed comparison of the wings of Hβ and [O III] because of the low-level contamination there by Fe II. Nevertheless after taking into account the known wavelengths of the Fe II lines, in particular Fe II λ4923, which contaminates the blue wing of [O III] λ4959, and Fe II λ5018, which is of similar strength, it is clear that Hβ emission is present up to -5000 km s^{-1} in its blue wing, whereas [O III] does not possess such a component. The blue wing of the stronger [O III] λ5007 line falls nearly to zero only -1900 km s^{-1} from its peak.

The values of FWHM listed in Table 1 are significantly smaller than those reported by Elizalde & Steiner (1994), and even slightly smaller than those given by Moran et al. (1996). This is a result of the better spectral resolution achieved here. IRAS 20181−2244 resembles most I Zw 1 objects in that its lines do not allow a clear separation between broad and narrow components. The permitted lines rise smoothly to a sharp cusp; consequently with better spectral resolution, a smaller FWHM is measured. Still, there is ample evidence that the permitted and forbidden lines arise at least in part in different regions, both from their differing line profiles, and from the observation that the Hβ line is often more highly polarized than the [O III] lines in NLS1s in general (Goodrich 1989), and in IRAS 20181−2244 in particular (Kay et al. 1996). While the Hβ line in IRAS 20181−2244 is polarized, the polarized line profile is not broader than the raw flux profile. Thus, there is no evidence for a hidden broad-line region in IRAS 20181−2244 similar to that in NGC 1068 and other Seyfert 2 galaxies.

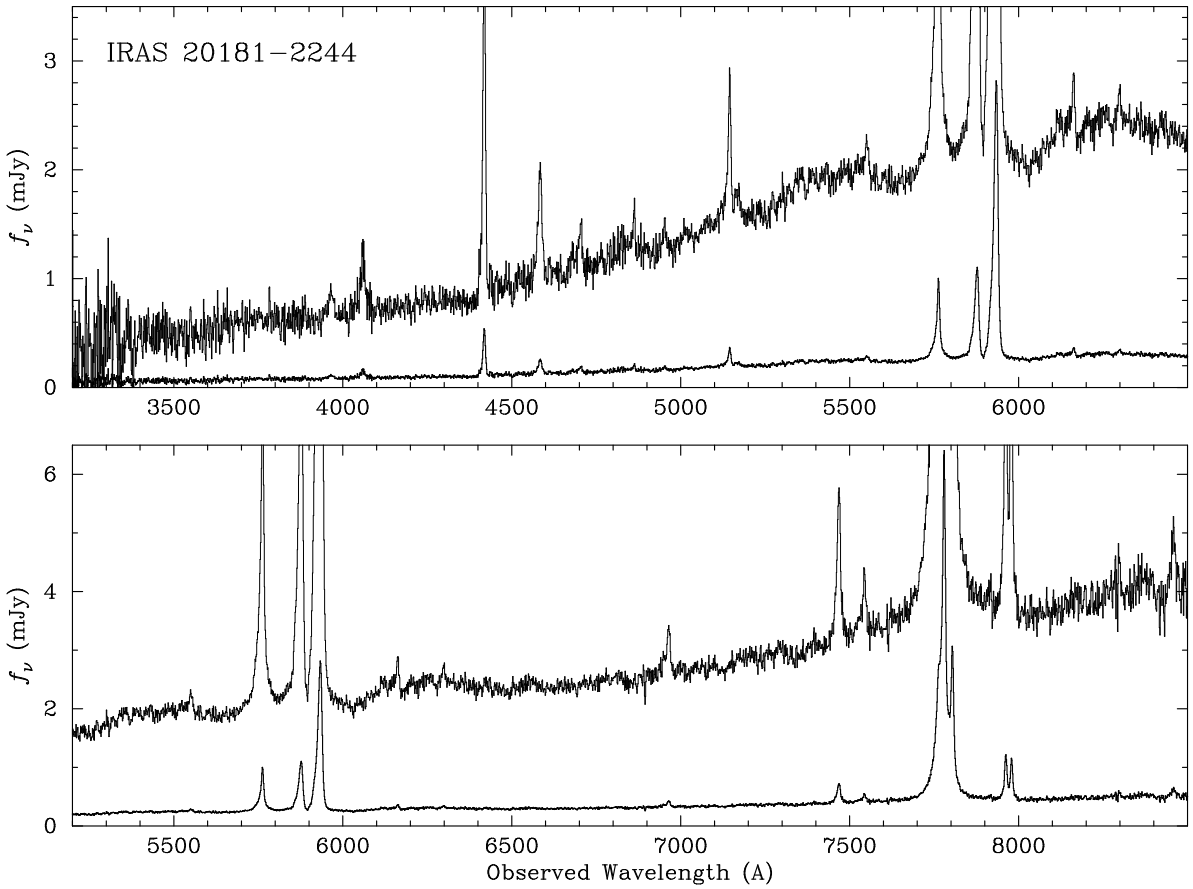

FIG. 2.—Spectrum of IRAS 20181−2244 from the KPNO 2.1 m telescope. Flux scale refers to the lower trace. The upper trace is the same spectrum multiplied by a factor of 8.

TABLE 1

EMISSION-LINE MEASUREMENTS OF IRAS 20181−2244

Line Identification	Flux[a] $F/F(\mathrm{H}\beta)$	Intensity[b] $I/I(\mathrm{H}\beta)$	FWHM (km s^{-1})	z_{helio}
Mg II λ2798	<0.30	<0.39	...	...
[Ne V] λ3346	0.07	0.08	...	...
[Ne V] λ3426	0.16	0.19	...	0.18491
[O II] λ3727	0.59	0.67	420	0.18540
[Ne III] λ3869	0.25	0.28	...	...
[Ne III] λ3968, Hε	0.05	0.05	...	...
Hδ	0.04	0.04	...	...
Hγ	0.25	0.26	475	0.18537
[O III] λ4363	0.05	0.05	...	...
Fe II λ4570	0.70	0.72	...	...
He II λ4686	0.03	0.03	...	...
Hβ	1.00	1.00	460	0.18537
[O III] λ4959	1.07	1.06	710	0.18517
[O III] λ5007	3.46	3.41	695	0.18510
[N I] λ5199	0.04	0.04	...	...
He I λ5876	0.09	0.08	...	...
[O I] λ6300	0.25	0.22	435	0.18534
[O I] λ6363	0.08	0.07	...	...
[N II] λ6548	0.21	0.19	...	...
Hα	7.52	6.65	465	0.18536
[N II] λ6583	0.64	0.57	...	0.18531
He I λ6678	0.03	0.02	...	...
[S II] λ6716	0.37	0.33	305	0.18542
[S II] λ6731	0.33	0.29	295	0.18543
[A III] λ7136	0.11	0.09	...	...

[a] Observed flux relative to $F(\mathrm{H}\beta) = 1.11 \times 10^{-14}$ ergs cm^{-2} s^{-1}.

[b] Intensity corrected for Galactic $E(B-V) = 0.12$ mag, relative to $I(\mathrm{H}\beta) = 1.43 \times 10^{-14}$ ergs cm^{-2} s^{-1}.

The reason Elizalde & Steiner (1994) first classified IRAS 20181−2244 optically as a type 2 QSO, analogous to, but more luminous than, NGC 1068, is that their spectrum did not have the resolution and signal-to-noise ratio to detect any of the I Zw 1 features described above. An additional improvement in our spectrum that is relevant to its classification can be seen in the deblending of its Hα and [N II] lines. By carefully correcting the atmospheric *A*-band contamination at 7600 Å, which falls on the wing of Hα, and by

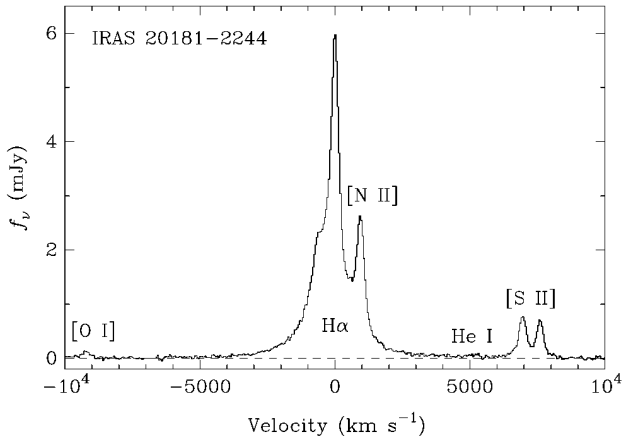

FIG. 3.—Continuum subtracted spectrum of IRAS 20181−2244 in velocity units. Broad Hα emission is present up to ±5000 km s^{-1}.

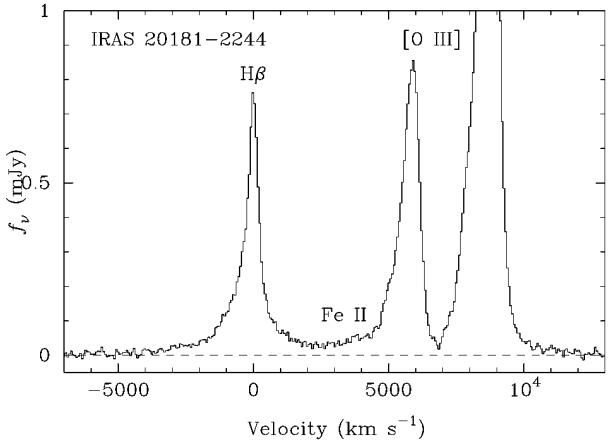

FIG. 4.—Continuum subtracted spectrum of IRAS 20181−2244 in velocity units. Hβ emission extends to ≈ −5000 km s^{-1}, while similar wings are not present in [O III] λλ4959, 5007. An apparent blue wing on [O III] λ4959 is probably due to Fe II λ4923.

requiring Hα to have a profile similar to that of Hβ, we see that the [N II] λλ6548, 6583 lines contribute only about 10% of the flux of the Hα, [N II] blend. In contrast, Elizalde & Steiner (1994) thought that the [N II] lines comprised almost half the flux of the blend, which would have supported classification as a type 2 QSO. Our larger Hα flux measurement, in addition to favoring a I Zw 1 classification, also increases the inferred value of the intrinsic extinction, which will become important in the interpretation of the X-ray spectrum presented in § 3.

Just about the only property of IRAS 20181−2244 that does *not* support the I Zw 1 classification is its [O III] λ5007/Hβ flux ratio of 3.4. Although violating the conventional upper limit of 3 on the [O III]/Hβ ratio of I Zw 1 objects, it would be pedantic to insist, in the face of all the evidence to the contrary, that IRAS 20181−2244 is a type 2 QSO just because its [O III]/Hβ ratio is 3.4 instead of 3.0. Therefore, despite this anomaly, we stand by our I Zw 1 classification, which we will support in the next section with further evidence from our *ASCA* observation. Then in § 4, we discuss the line and continuum properties of IRAS 20181−2244 in comparison with the 19 other I Zw 1 objects found in the Boller et al. (1992) sample and show how IRAS 20181−2244 finds its natural place among them.

3. *ASCA* X-RAY OBSERVATION

IRAS 20181−2244 was observed by *ASCA* on 1995 October 11–13. Data obtained with the four instruments on board *ASCA* were filtered following the standard procedures described in *The ABC Guide to ASCA Data Reduction.* The SIS detectors were operated in 1-CCD mode, with the target placed at the default 1-CCD position. Source counts in the SIS images were extracted using a 3′ radius circular region, and background counts were collected from the entire chip, excluding a 4′ radius region centered on the target. In the GIS images, source counts were extracted using a region of 6′ in radius. The GIS background was measured in a source-free part of the image located the same distance off-axis as IRAS 20181−2244 with twice the area of the region used to extract the target. Useful exposure times and average background-subtracted source count rates in the four ASCA detectors are listed in Table 2. We combined the two SIS spectra and the two GIS

TABLE 2

ASCA OBSERVATION SUMMARY

Instrument	Exposure Time (s)	Count Rate (0.5–10 keV) (s^{-1})
SIS0	51,284	5.97×10^{-2}
SIS1	50,724	4.94×10^{-2}
GIS2	58,222	3.41×10^{-2}
GIS3	58,216	4.26×10^{-2}

spectra using the FTOOLS software task "addascaspec." For spectral fitting, the SIS and GIS spectra were rebinned to have at least 100 counts (source plus background) per channel.

3.1. *X-Ray Spectral Fitting*

A simple model consisting of a single absorbed power law provides a fully adequate fit to the 0.5–8 keV *ASCA* spectrum of IRAS 20181−2244, as Figure 5 and Table 3 indicate. Because it is clear from preliminary spectral fitting that an absorbing column density significantly larger than the Galactic value of $N_H = 7.4 \times 10^{20}$ cm^{-2} is required, we included the latter as a fixed parameter and fitted for an additional, intrinsic N_H at the redshift of 0.185. Separate and simultaneous fits to the SIS GIS spectra yield similar spectral parameters and model normalizations. For the simultaneous fit, the derived power-law photon index ($\Gamma = 2.37 \pm 0.09$ at 90% confidence) and intrinsic column density ($N_H = 1.6^{+0.5}_{-0.4} \times 10^{21}$ cm^{-2}) are well constrained, as the confidence contours displayed in Figure 6 demonstrate. Using this model and the average power-law normalization of $A = 7.8 \times 10^{-4}$ photons cm^{-2} s^{-1} keV^{-1}, we measure fluxes of 1.00×10^{-12} and 1.15×10^{-12} ergs cm^{-2} s^{-1} in the observed 0.5–2 keV and 2–10 keV ranges, respectively. The model implies an unabsorbed luminosity for IRAS 20181−2244 of $L_X = 3.3 \times 10^{44}$ ergs s^{-1} in the rest-

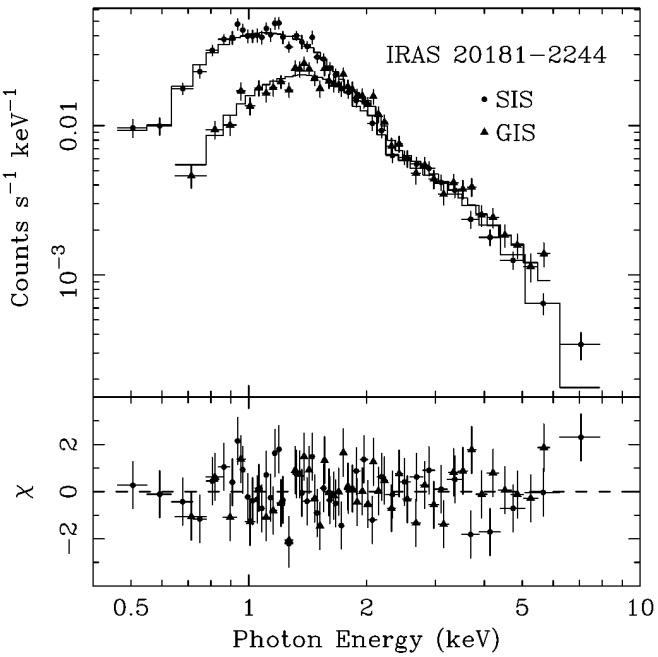

FIG. 5.—Observed *ASCA* SIS (*filled circles*) and GIS (*filled triangles*) spectra of IRAS 20181−2244 and best-fit power-law model ($\Gamma = 2.37$, intrinsic $N_H = 1.6 \times 10^{21}$ cm^{-2}).

TABLE 3

POWER-LAW FITS TO THE *ASCA* SPECTRA OF IRAS 20181−2244

Instruments	Energy Range (keV)	Γ	N_H[a] (10^{21} cm^{-2})	A_{SIS}/A_{GIS}[b]	χ^2 (dof)
SIS + GIS.....	0.5–8	$2.37^{+0.09}_{-0.09}$	$1.6^{+0.5}_{-0.4}$	7.4/8.1	85.1 (85)
SIS	0.5–8	$2.42^{+0.11}_{-0.11}$	$1.7^{+0.5}_{-0.5}$	7.6	44.2 (41)
GIS	0.7–6	$2.34^{+0.22}_{-0.19}$	$2.0^{+2.0}_{-1.9}$	8.2	37.9 (42)
SIS + GIS.....	0.5–2	$2.34^{+0.21}_{-0.22}$	$1.5^{+0.6}_{-0.6}$	7.3/8.0	57.2 (58)
SIS + GIS.....	2–8	$2.39^{+0.11}_{-0.11}$	1.6[c]	7.5/8.4	34.3 (36)

[a] Column density intrinsic to IRAS 20181−2244, in addition to the Galactic column of 7.4×10^{20} cm^{-2}.

[b] Power-law normalization at 1 keV, in units of 10^{-4} photons cm^{-2} s^{-1} keV^{-1}.

[c] Fixed parameter.

frame 0.5–2 keV band, and $L_X = 5.5 \times 10^{44}$ ergs s^{-1} in the rest-frame 0.5–10 keV band.

The spectral index $\Gamma = 2.37$ is typical for NLS1s, the X-ray spectra of which are generally steeper than those of ordinary Seyfert 1 galaxies (Boller, Brandt, & Fink 1996; Brandt, Mathur, & Elvis 1997; Forster & Halpern 1996). Fits above and below 2 keV, as listed in Table 3, reveal that the spectrum of IRAS 20181−2244 is similarly steep in both the hard and soft bands.

It is noteworthy that the derived column density of $N_H = 1.6^{+0.5}_{-0.4} \times 10^{21}$ cm^{-2}, while unlike the very large obscuration that is seen by *ASCA* in some Seyfert 2 galaxies, is nevertheless significantly larger than a typical Seyfert 1 or QSO value. In view of the moderately large Hα/Hβ ratio of 6.65 which we measure after dereddening by the Galactic extinction, it is plausible that general obscuration in the host galaxy of IRAS 20181−2244 is responsible for both its additional X-ray absorption and its large Balmer decrement. An additional extinction $E(B-V) \simeq 0.32$ mag intrinsic to IRAS 20181−2244 would be consistent with its low-energy X-ray spectral cutoff and would reduce its true Balmer decrement to 4.7, a value more similar to the broad-line decrements of unreddened QSOs.

This moderate column density also helps to explain the relatively weak detection of IRAS 20181−2244 as a soft X-ray source in the *ROSAT* all-sky survey. An extrapolation of the absorbed *ASCA* spectrum to softer energies predicts a *ROSAT* count rate of 0.091 counts s^{-1}, while the observed rate was 0.060 counts s^{-1} (Boller et al. 1992). The same X-ray continuum, if absorbed by only the Galactic column of $N_H = 7.4 \times 10^{20}$ cm^{-2}, would have yielded 0.149 counts s^{-1} in *ROSAT*. Of course, a direct comparison of noncontemporaneous *ROSAT* and *ASCA* measured fluxes is of limited value because I Zw 1 objects often display large-amplitude variability in the long term (e.g., Forster & Halpern 1996), which may be as much responsible for the weaker *ROSAT* flux as is intrinsic absorption.

3.2. *X-Ray Variability*

The binned four-instrument *ASCA* light curve of IRAS 20181−2244 is displayed in Figure 7. IRAS 20181−2244 is clearly a variable X-ray source, with intensity fluctuations in excess of a factor of 2 on a timescale of a few hours. This variability convincingly rules out the hidden/scattered QSO hypothesis for IRAS 20181−2244 since in that scenario, the large size of the region responsible for scattering radiation in our direction would average out any intrinsic short-term variability of the compact source. On the other hand, rapid X-ray variability is a common property of I Zw 1 objects (Forster & Halpern 1996, and references therein), which

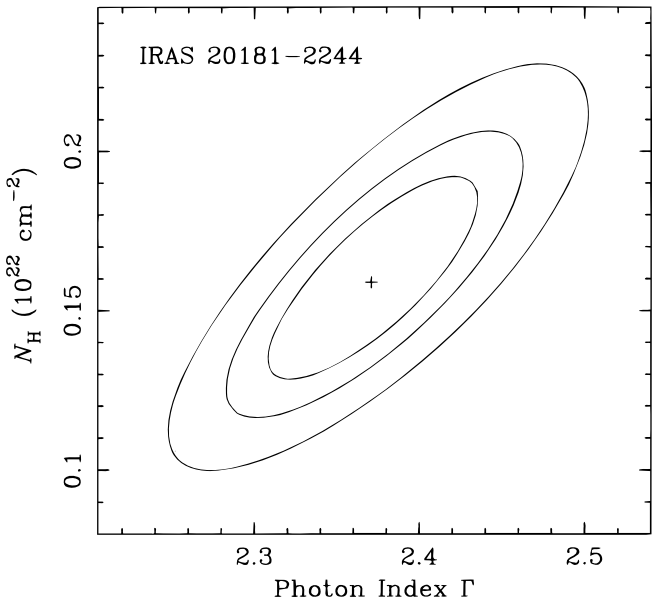

FIG. 6.—Confidence contours for the parameters of the power-law model fitted jointly to the SIS and GIS spectra. Contours are 68%, 90%, and 99% confidence limits for two interesting parameters.

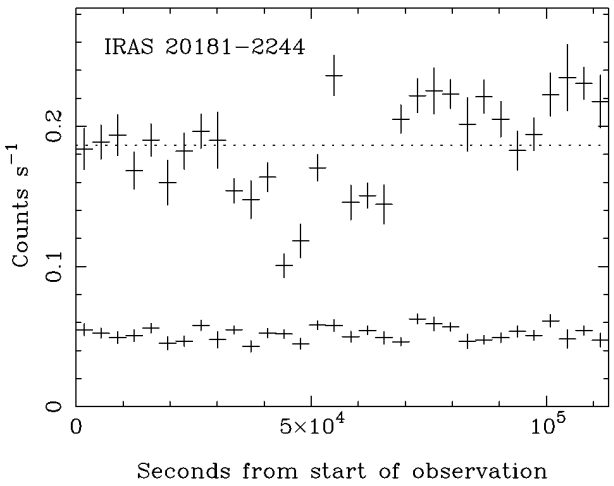

FIG. 7.—The 0.5–8 keV background-subtracted *ASCA* light curve of IRAS 20181−2244 in 1 hr bins. Dotted line represents the mean total count rate, and temporal variations in the background are indicated with the lower set of crosses. Light curves were constructed for each of the four *ASCA* instruments, properly correcting for the actual time spent on-source in each interval. Individual count rates, and their associated variances, were then summed to produce the composite light curve displayed here.

further supports our I Zw 1 classification of IRAS 20181−2244. The fastest variability in Figure 7 can be characterized as a doubling of flux in two hours. If this variation is spectrally independent across the 0.5–10 keV band, it corresponds to $\Delta L/\Delta t = 7.6 \times 10^{40}$ ergs s^{-2}. According to Fabian (1979), the efficiency η for an isotropic source powered by accretion must be greater than $5 \times 10^{-43} \Delta L/\Delta t$. For IRAS 20181−2244, $\eta > 0.038$, which is large, but not as large as some of the more extreme values seen in NLS1s, which can exceed 0.10. Extreme nonlinear variability seems to be a characteristic property of I Zw 1 objects as seen by *ASCA* (Leighly et al. 1997a), and it is interesting to speculate that the real efficiency of IRAS 20181−2244 might be considerably higher if its variability encompasses soft X-ray or EUV flux below the observable bandpass, or if more dramatic flaring behavior occurs at times when we are not watching.

4. DISCUSSION

4.1. *IRAS 20181–2244 among the I Zw 1 Class*

As discussed in § 2, the optical emission-line spectrum of IRAS 20181−2244 conforms well enough to the populous I Zw 1 class that we find little reason to invoke the more exotic possibility of a "type 2 QSO." We can further evaluate its membership credentials by comparing its continuum and emission-line properties with those of the 19 other *ROSAT*/*IRAS* selected objects that Moran et al. (1996) assigned to the I Zw 1 class. This is a sample of substantial size and uniform selection criteria. We draw upon the data in Tables 2 and 4 of Moran et al. (1996) to produce Figure 8, a display of the basic properties of *ROSAT*/*IRAS*-selected I Zw 1 objects.

It has long been known that I Zw 1 objects can be highly luminous, both as infrared and X-ray sources. The average continuum luminosity (and average redshift) of I Zw 1 objects is well above that of all other types of Seyfert galaxies in the *ROSAT*/*IRAS* survey. The far-infrared luminosities of several of these exceed $10^{12}\ L_\odot$, and their X-ray luminosities are proportionally high as well. While IRAS 20181−2244 is among the more luminous ones in X-rays and infrared, its continuum luminosity is not outstanding in any way. Many of the PG quasars also fall into the I Zw 1 class, as shown by the spectra of Boroson & Green (1992). Unlike Seyfert 2 galaxies, I Zw 1 objects seem not be limited to low luminosity. As exemplified by highly luminous QSOs like PHL 1092 (Forster & Halpern 1996), it appears that no useful distinction is to be made between I Zw 1 objects of Seyfert-like and QSO-like luminosity.

In terms of emission-line properties, IRAS 20181−2244 is near the low end in FWHM and Fe II/Hβ ratio, but not uniquely so. The only property that distinguishes IRAS

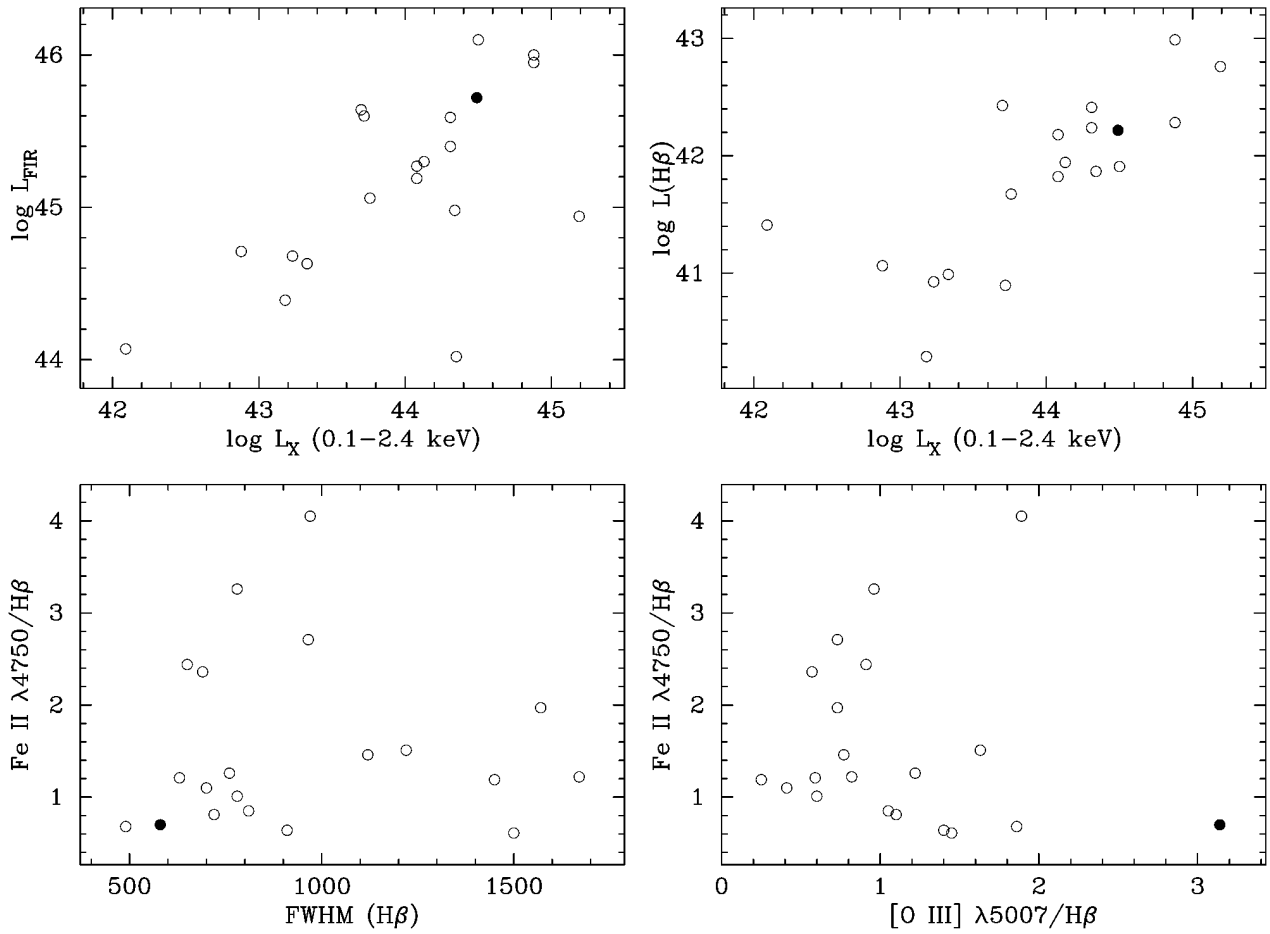

FIG. 8.—Comparison of continuum and emission-line properties of the 20 *ROSAT*/*IRAS*–selected I Zw 1 objects. Data are drawn from Tables 2 and 4 of Moran, Halpern, & Helfand (1996). Filled circle denotes IRAS 20181−2244. Note that its emission-line measurements, taken from Moran et al. (1996) for this figure, differ slightly from those listed in Table 1; this is because the spectrum reported in this paper is of somewhat better resolution than those obtained for the entire Moran et al. sample.

20181−2244 in Figure 8 is its [O III]/Hβ ratio, which is slightly greater than 3. Given all the other supporting evidence discussed above, we consider this one anomaly insufficient grounds to abandon our I Zw 1 interpretation.

4.2. *Are There Any Type 2 QSOs?*

Having stricken IRAS 20181−2244 from the short list of candidates that are occasionally nominated for the honor of type 2 QSO, it remains for us to ask if there are *any* such objects. That is, are there any high-luminosity counterparts of Seyfert 2 galaxies. Forster & Halpern (1996) recently addressed this question with regard to the handful of such X-ray selected objects, offering a generally pessimistic evaluation of the qualifications of the proposed candidates and eliminating all but three from active consideration. In the short time since that assessment was offered, new evidence has come to light that disqualifies two of the remaining contenders. First, the *ROSAT* source RX J13434+0001 at $z = 2.35$, proposed by Almaini et al. (1995) as a type 2 QSO on the basis of its narrow Lyα and C IV emission lines, was quickly shown by the same group of authors to have a quite ordinary broad Hα line in an infrared spectrum (Shanks et al. 1996). Thus, it is a moderately reddened but otherwise ordinary QSO. Second, Halpern, Eracleous, & Forster (1998) have obtained spectra of the "original" narrow-line QSO, 1E 0449−184 at $z = 0.338$ (Stocke et al. 1982; Stephens 1989), showing that all three of its Mg II, Hβ, and Hα lines actually have broad components of substantial strength. (Although Stocke et al. 1983 detected a broad Mg II line in 1E 0449−184 shortly after their original discovery, their second paper is rarely referenced in discussions of this subject, and 1E 0449−184 is often referred to as a narrow-line QSO without qualification.) In fact, there remains only one very faint emission-line object, the *ASCA* source AX J08494+4454 at $z = 0.9$ (Ohta et al. 1996), that is still claimed to be a type 2 QSO. In view of its faintness we consider this object to be no stronger a candidate than the others. At the time of this writing, there is a dearth of evidence for the existence of *any* type 2 QSO among X-ray detected AGNs.

Of course, in the standard unified scheme there are no *true* Seyfert 2 galaxies, only Seyfert 1s hidden by molecular tori. In the unified scheme, the absence of type 2 QSOs among X-ray selected samples is natural if either (1) the X-rays from all such objects are hidden from view, or (2) all sufficiently luminous QSO nuclei are able to remove any obscuring dust from their vicinity, allowing their broad-line regions to be visible from any direction. Although a number of ultraluminous *IRAS* galaxies have Seyfert 2 spectra and hidden broad-line regions (e.g., Wills & Hines 1997, and references therein), there is not much evidence that they harbor *luminous* X-ray sources. While both of the explanations offered above for this absence may be responsible to some degree, there are counterexamples to either. First, a substantial number of Seyfert 2 galaxies *are* detected in hard X-rays becuse their column densities, in the range 10^{23}–10^{24} cm^{-2}, are not so large as to be completely opaque (e.g., Awaki et al. 1991; Salvati et al. 1997). Second, even objects of modest quasar-like luminosity, principally radio galaxies like Cygnus A, are able to retain their obscuring material while permitting their broad Mg II emission lines to be visible in (Rayleigh) scattered light (Antonucci, Hurt, & Kinney 1994). A power-law nuclear X-ray source with 2–10 keV luminosity of $\sim 1 \times 10^{45}$ ergs s^{-1} was detected in Cygnus A by *Ginga* (Ueno et al. 1994). So it seems that the obscuring gas and dust that is essential to the unified scheme is neither so substantial as to prevent direct X-ray detection or indirect UV scattering, nor so fragile as to be destroyed in the QSO environment. Thus, the absence of type 2 X-ray sources of higher luminosity, and the rarity of type 2 QSOs compared to ordinary QSOs, remain significant facts to be explained whether in the context of unified models or not. The two commonly offered explanations mentioned at the beginning of this paragraph, while having considerable promise, could both use additional detailed evaluation. In particular, it seems that further observations and analysis of existing X-ray surveys could end up favoring one explanation over the other.

4.3. *So What Are I Zw 1 Objects Anyway?*

In this paper we have been concerned primarily with establishing by a preponderance of evidence that IRAS 20181−2244 belongs among the well populated I Zw 1 objects. Although the logic behind the designation of such a class was recognized long ago on the basis of emission-line widths and ratios alone (Osterbrock & Pogge 1985; Goodrich 1989), it is only recently that a wider range of properties have been discovered that affirm the distinctive nature of these objects. Among these are steep optical and X-ray spectra in comparison with normal type 1 and 2 Seyferts, rapid and/or large amplitude X-ray variability (e.g., Boller et al. 1996; Grupe et al. 1995a, 1995b; Forster & Halpern 1996; Otani, Kii, & Miya 1996; Brandt et al. 1997; Boller et al. 1997; Leighly et al. 1997a), and possible association with broad absorption line QSOs (Boroson & Meyers 1992; Lawrence et al. 1997; Leighly et al. 1997b, 1997c).

While it is fairly clear that this ensemble of properties eludes explanation within the Seyfert unification paradigm, a robust physical model for the special properties of I Zw 1 objects is not obviously forthcoming. Motivated by the extremely high efficiencies implied by rapid X-ray variability, generic explanations involving Eddington-limited accretion onto a black hole of smaller than average mass, or onto a Kerr black hole, have been offered (Pounds, Done, & Osborne 1995; Puchnarewicz et al. 1995; Forster & Halpern 1996). The smaller mass might allow the tail of thermal emission from an accretion disk to extend into the soft X-rays, producing the very steep spectra seen by *ROSAT*. At the same time, these abundant soft photons might Compton cool to a greater degree the hot plasma that is needed to produce the hard X-ray power law, thus steepening the emitted hard X-ray spectrum. In this scenario, the narrower emission lines of I Zw 1 objects could perhaps be attributed to their smaller black-hole masses, although it is not obvious why.

One possible scenario involves the concept of "locally optimally emitting clouds" (Baldwin et al. 1995), in which clouds with a large range of densities and distances tend to emit individual lines at preferred values of the ionization parameter. If the emitting clouds are gravitationally bound, then their velocity is proportional to $M_{\rm BH}^{1/2}(nU/L)^{1/4}$, where U is the ionization parameter. Assuming fixed density n and ionization parameter U, velocity scales as $M_{\rm BH}^{1/4}(L/L_{\rm Edd})^{-1/4}$. Small line width would be favored by either a small mass or a high accretion rate. The weak dependence of velocity on these parameters is consistent with the small range, perhaps a factor of 10, in the line widths of Seyfert 1 galaxies and QSOs. It is not clear how the emission-line *ratios* of I Zw 1

objects, in particular their strong Fe II, would be explained in this picture. But it may have something to do with the steep ionizing continuum that favors soft X-ray and EUV photons. Detailed photoionization calculations using these extreme continuum shapes are certainly needed.

Alternative ideas, involving particular viewing directions, are sometimes invoked to explain the narrow emission-line widths. These scenarios rely on a "pole-on" geometry (Osterbrock & Pogge 1985; Puchnarewicz et al. 1992), but this implies an assumption about the velocity field of the emission-line clouds that has little or no independent support. Although a viewing angle face on to an accretion disk will likely affect the shape of the continuum spectrum observed, given the variety of plausible accretion disk structures it is far from clear what the quantitative effect is, and even less so that X-ray variability should appear more extreme from this direction. So we judge that our theoretical understanding of the I Zw 1 phenomenon lags pretty far behind the observations. Despite our current inability to come up with a convincing explanation for all the extreme properties of I Zw 1 objects, we are compelled to believe that they offer us important new clues to the physics of active galactic nuclei in general.

This work was supported at Columbia by a grant from NASA under the *ASCA* Guest Investigator Program (NAG 5-2524) and at the Lawrence Livermore National Laboratory by the US Department of Energy under contract W-7405-ENG-48. This paper is contribution 636 of the Columbia Astrophysics Laboratory.

REFERENCES

Almaini, O., Boyle, B. J., Griffiths, R. E. Shanks, T., Stewart, G. C., & Georgantopoulos, I. 1995, MNRAS, 277, L31
Antonucci, R., Hurt, T., & Kinney, A. 1994, Nature, 371, 313
Awaki, H., Koyama, K., Inoue, H., & Halpern, J. P. 1991, PASJ, 43, 1995
Baldwin, J., Ferland, G., Korista, K., & Verner, D. 1995, ApJ, 455, L119
Boller, T., Brandt, W. N., Fabian, A. C., & Fink, H. 1997, MNRAS, 289, 393
Boller, T., Brandt, W. N., & Fink, H. 1996, A&A, 305, 53
Boller, T., Meurs, E. J. A., Brinkmann, W., Fink, H., Zimmermann, U., & Adorf, H.-M. 1992, A&A, 261, 57
Boroson, T. A., & Green, R. F. 1992, ApJS, 80, 109
Boroson, T. A., & Meyers, K. A. 1992, ApJ, 397, 442
Brandt, W. N., Mathur, S., & Elvis, M. 1997, MNRAS, 285, 25
Elizalde, F., & Steiner, J. E. 1994, MNRAS, 268, L47
Fabian, A. C. 1979, Proc. R. Soc. London A, 366, 449
Forster, K., & Halpern, J. P. 1996, ApJ, 468, 565
Goodrich, R. W. 1989, ApJ, 342, 234
Grupe, D., Beuermann, K., Mannheim, K., Bade, N., Thomas, H.-C., de Martino, D., & Schwope, A. 1995a, A&A, 299, L5
Grupe, D., Beuermann, K., Mannheim, K., Thomas, H.-C., Fink, H. H., & de Martino, D. 1995b, A&A, 300, L21
Halpern, J. P., Eracleous, M., & Forster, K. 1998, ApJ, submitted
Kay, L., Magalhães, M., Elizalde, F., & Rodrigues, C. 1996, BAAS, 28, 914
Lawrence, A., Elvis, M., Wilkes, B. J., McHardy, I., & Brandt, N. 1997, MNRAS, 285, 879
Leighly, K., M., et al. 1997a, ApJ, in preparation
Leighly, K. M., Mushotzky, R. F., & Nandra, K. 1997b, in ASP Conf. Ser. 128, Mass Ejection from AGNs, ed. N. Arav, I. Schlosman, & R. Weymann (San Francisco: ASP), 155
Leighly, K. M., Mushotzky, R. F., Nandra, K., & Forster, K. 1997c, ApJ, 489, L25
Moran, E. C., Halpern, J. P., & Helfand, D. J. 1996, ApJS, 106, 341
Ohta, K., Yamada, T., Nakanishi, K., Ogasaka, Y., Kii, T., & Hayashida, K. 1996, ApJ, 458, L57
Osterbrock, D. E., & Pogge, R. W. 1985, ApJ, 297, 166
Otani, C., Kii, T., & Miya, K. 1996, in Röntgenstrahlung from the Universe, ed. H. U. Zimmermann, J. E. Trümper, & H. Yorke (Garching: MPE Rep. 263), 491
Phillips, M. M. 1976, ApJ, 208, 37
Pounds, K. A., Done, C., & Osborne, J. 1995, MNRAS, 277, L5
Puchnarewicz, E. M., Mason, K. O., Córdova, F. A., Kartje, J., Branduardi-Raymont, G., Mittaz, J. P. D., Murdin, P. G., & Allington-Smith, J. 1992, MNRAS, 256, 589
Puchnariewicz, E. M., Mason, K. O., Siemiginowska, A., & Pounds, K. A. 1995, MNRAS, 276, 20
Salvati, M., Bassani, L., Della Ceca, R., Maiolino, R., Matt, G., & Zamorani, G. 1997, A&A, 323, L1
Shanks, T., et al. 1996, in Röntgenstrahlung from the Universe, ed. H. U. Zimmermann, J. E. Trümper, & H. Yorke (Garching: MPE Rep. 263), 341
Stark, A. A., Gammie, C. F., Wilson, R. W., Bally, J., Linke, R. A., Heiles, C., & Hurwitz, M. 1992, ApJS, 79, 77
Stephens, S. A. 1989, AJ, 97, 10
Stocke, J. T., Liebert, J., Gioia, I. M., Griffiths, R. E., Maccacaro, T., Danziger, I. J., Kunth, D., & Lub, J. 1983, ApJ, 273, 458
Stocke, J., Liebert, J., Maccacaro, T., Griffiths, R. E., & Steiner, J. E. 1982, ApJ, 252, 69
Ueno, S., Koyama, K., Nishida, M., Yamauchi, S., & Ward, M. J. 1994, ApJ, 431, L1
Wills, B. J., & Hines, D. C. 1997, in ASP Conf. Ser. 128, Mass Ejection from AGNs, ed. N. Arav, I. Schlosman, & R. Weymann (San Francisco: ASP), 99